IEEE Robotics and Automation Letters (RA-L) paper, presented at ICRA 2026, Vienna, Austria. Cite as RA-L paper.

Understanding Lidar Variability: A Dataset and Comparative Study Featuring Dome-Shaped, Solid-State, and Spinning Lidars

Doumegna Mawuto Koudjo Felix*, Xianjia Yu*, Jiaqiang Zhang, Sier Ha, Zhuo Zou, Tomi Westerlund

***Abstract*—Lidar technology has been widely employed across various applications, such as robot localization in GNSS-denied environments and 3D reconstruction. Recent advancements have introduced different lidar types, including cost-effective solid-state lidars such as the Livox Avia and Mid-360. The Mid-360, with its dome-like design, is increasingly used in portable mapping and unmanned aerial vehicle (UAV) applications due to its low cost, compact size, and reliable performance. However, the lack of datasets that include dome-shaped lidars, such as the Mid-360, alongside other solid-state and spinning lidars significantly hinders the comparative evaluation of novel approaches across platforms. Additionally, performance differences between low-cost solid-state and high-end spinning lidars (e.g., Ouster OS series) remain insufficiently examined, particularly without an Inertial Measurement Unit (IMU) in odometry.**

To address this gap, we introduce a novel dataset comprising data from multiple lidar types, including the low-cost Livox Avia and the dome-shaped Mid-360, as well as high-end spinning lidars such as the Ouster series. Notably, to the best of our knowledge, no existing dataset comprehensively includes dome-shaped lidars such as Mid-360 alongside both other solid-state and spinning lidars. In addition to the dataset, we provide a benchmark evaluation of state-of-the-art SLAM algorithms applied to this diverse sensor data. Furthermore, we present a quantitative analysis of point cloud registration techniques, specifically point-to-point, point-to-plane, and hybrid methods, using indoor and outdoor data collected from the included lidar systems. The outcomes of this study establish a foundational reference for future research in SLAM and 3D reconstruction across heterogeneous lidar platforms.

***Index Terms*—Localization; SLAM; Data Sets for SLAM;**

I. Introduction

LIDAR has become a critical technology in robotics and 3D reconstruction applications. It significantly enhances robotic perception when integrated with other sensors, including conventional cameras, event cameras, inertial measurement units (IMUs), and various other sensory devices [1], [2], [3]. In particular, lidar has emerged as one of the primary sensors for robot localization in GNSS-denied or unreliable environments. In such scenarios, it is commonly used together, significantly improved by, and dependent on IMU [2], [4].

In recent years, lidar technology has evolved considerably for high-end models and more cost-effective alternatives. Traditional spinning lidars typically use a rotating mechanism to continuously scan the environment with a laser beam, producing a 360° point cloud over time. However, solid-state lidars employ no moving parts and instead rely on electronic beam steering or flash illumination to capture depth information. This results in more compact, robust, and energy-efficient designs, albeit often with a narrower field of view (FoV). Livox lidars have garnered increasing attention among various solid-state lidar technologies due to their unique non-repetitive scanning patterns and cost-effective designs [5], [2]. These Livox sensors provide varying FoVs, such as the Livox Avia, which has a limited FoV, and the Livox Mid-360, which features a dome-shaped design. The latter, in particular, offers a cost-effective yet accurate solution for 3D lidar-based simultaneous localization and mapping (SLAM). Notably, the Livox Mid-360's unique design makes it highly suitable for various mapping applications. However, to the best of our knowledge, no existing dataset contains all these lidar types within a single data sequence, with all sensors mounted simultaneously on an identical platform.

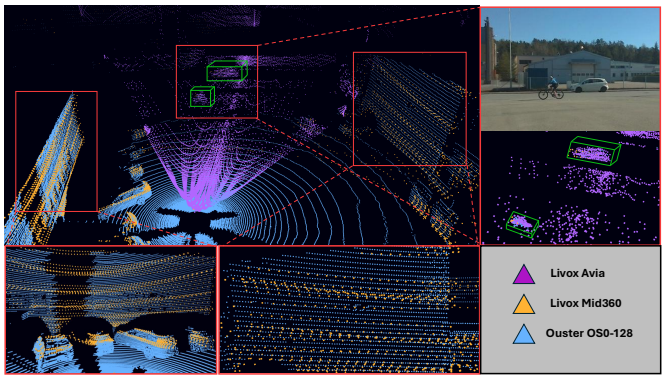

Fig. 1: The point cloud differences of the objects under three different types of lidars, including Livox Avia, Mid-360, and Ouster OS0-128.

Fig. 1 shows the point cloud differences of the same objects under different lidars. Studies have demonstrated that solid-state lidar systems like the Livox Mid-360 deliver competitive performance [5]. Despite these advancements, they typically exhibit a more irregular scanning pattern and sometimes lower resolution than high-end spinning models. These lidar data characteristics (i.e., density, resolution, and scanning pattern) may potentially affect the accuracy of odometry in differ-

Manuscript received: July 10th, 2025; Revised: October 5th, 2025; Accepted: November 11th, 2025.

This paper was recommended for publication by Editor Javier Civera upon evaluation of the Associate Editor and Reviewers' comments.

* These authors contributed equally to this work. (Corresponding author: Xianjia Yu)

This research is supported by the Research Council of Finland's Digital Waters (DIWA) flagship (Grant No. 359247).

Doumegna Mawuto Koudjo Felix and Zhuo Zou are also with School of Information Science and Technology, Fudan University, Shanghai, China, e-mails::{23210720352, zhuo}@m.fudan.edu.cn.)

The authors are with Turku Intelligent Embedded and Robotic Systems (TIERS) Lab, University of Turku, Turku, Finland, e-mails: {mawuto.k.doumegna, xianjia.yu, jiaqiang.zhang, sierha, zhuo.zuo, tovewe}@utu.fi.)

Digital Object Identifier (DOI): see top of this page.

IEEE Robotics and Automation Letters (RA-L) paper, presented at ICRA 2026, Vienna, Austria. Cite as RA-L paper.

ent types of environments accordingly. However, nowadays, lidar-based odometry (Lidar-Inertial Odometry, LIO) is highly dependent on IMUs. It is challenging and lacks independent research on the influence that these lidar features will bring into the point cloud registration or matching, particularly for different types of point cloud registration techniques, such as point-to-point and point-to-plane methods, in the absence of IMU assistance for forward propagation remains unclear.

To address this gap, this study introduces a novel dataset alongside qualitative benchmark and analysis. The findings of this study are intended to provide a valuable reference for researchers and practitioners in the field. The main contributions of this paper are as follows:

i). Dataset creation: We present the first state-of-the-art dataset where every single data sequence integrates multiple types of lidar sensors, including spinning, solid-state, and dome-shaped lidars, with a motion capture (MoCap) system or GNSS/RTK, thereby providing highly accurate odometry ground truth. The dataset was collected across a diverse range of scenarios, including both indoor and outdoor environments.

ii). Understanding lidar variability (LIO): We benchmark the performance of state-of-the-art SLAM methods on different lidar data collected in the proposed dataset, establishing baseline performance to facilitate a deeper understanding of the differences among these lidar types.

iii). Understanding lidar variability (point cloud match): To eliminate reliance on the IMU, we evaluate the performance of point clouds generated by different types of lidar sensors. The registration methods considered include point-to-point, point-to-plane, and their hybrid variants.

The remainder of this document is organized as follows: Section II introduces the recent development of lidars, their datasets, the state-of-the-art SLAM and point cloud matching methods. Section III then describes this study's methodology. Section IV presents the experimental results, while Section V concludes the work and outlines directions for future research.

II. Related Work

A. Advancement of Lidars

Lidar technology has seen significant advancements in recent years, leading to the development of high-end spinning lidars and more affordable solid-state options. Traditionally, spinning lidar sensors, such as those from Velodyne and Ouster, have dominated the market due to their high accuracy and wide FoV [6]. These sensors, commonly used in autonomous vehicles, typically operate at fixed frequencies (e.g., 10-20 Hz) and offer superior scanning capabilities thanks to their rotating laser scanners, which create detailed 3D maps of the environment. Beyond serving as a source for point cloud data, lidar can also generate images, where pixels are encoded by the intensity of the ambient light or reflected infrared light emitted by itself. This is more evident nowadays when the lidar resolution increases, such as with Ouster lidar. This presents a potential way for applying conventional computer vision methods to these lidar-generated images [7], [8], [9], [10].

In contrast, solid-state lidar systems, such as the Livox Avia and Livox Mid-360, have introduced substantial cost reductions, compactness, and increased adaptability for various applications [11]. The Livox Mid-360 is particularly noteworthy for its unique dome-shaped design, which provides a 360° horizontal FoV and a vertical range of approximately 25°. This design enables a more compact solution, making it suitable for portable mapping systems, unmanned aerial vehicles (UAVs), and robotic applications in GNSS-denied environments [12]. The Mid-360 is a cost-effective alternative for applications requiring less dense point clouds, such as SLAM in mobile robots and 3D reconstruction tasks [11].

Recent advancements in lidars have been more accessible, and developments in Livox sensors indicate promising improvements in point cloud density and overall performance. As lidars continue to diversify, the integration of various types of solid-state, spinning, and hybrid systems has paved the way for more comprehensive datasets that can serve as valuable resources for future research [6], [12].

These advancements also suggest the potential for further optimization in point cloud matching techniques. Research has concentrated on understanding how the specific characteristics of each lidar type impact the accuracy of 3D reconstructions. Despite technological progress, there is still a lack of datasets that comprehensively combine different lidar types for benchmarking point cloud matching performance.

B. Lidar Datasets

Lidar datasets are crucial for advancing point cloud processing, robotic localization, 3D reconstruction, and SLAM. Over the years, various datasets have been created for applications such as autonomous driving, mapping, and, urban modeling.

1) Existing State-of-the-Art Datasets: Most existing benchmark datasets predominantly focus on spinning lidar systems, exemplified by the widely used KITTI dataset [13] and the Oxford RobotCar dataset [14], both incorporating Velodyne HDL-64E spinning lidars. Similarly, datasets like ApolloScape [15] and Ouster's research datasets [16] emphasize high-resolution spinning systems. Although these resources have proven invaluable for research on SLAM and autonomous driving, they do not comprehensively address the broader spectrum of lidar sensor modalities. In particular, datasets combining spinning, solid-state, and dome-shaped lidars remain rare.

One notable advancement is the TIERS Multi-Modal Lidar Dataset [17], which includes Velodyne, Ouster OS-series, and Livox Avia sensors to support benchmarking general-purpose localization and mapping algorithms. While the TIERS dataset represents an essential step toward multi-modal sensor integration, it still lacks coverage of dome-shaped sensors such as the Livox Mid-360. This particular sensor's unique 360° horizontal field of view and approximately 25° vertical span make it especially suitable for portable mapping and UAV applications in GNSS-denied environments [18].

Recently, two additional datasets have emerged that attempt to tackle lidar-based odometry and registration challenges. The GEODE dataset [19] was developed to benchmark localization robustness in degenerate environments such as corridors and open spaces. Although GEODE includes heterogeneous lidar configurations and focuses on structure-scarce conditions, a

IEEE Robotics and Automation Letters (RA-L) paper, presented at ICRA 2026, Vienna, Austria. Cite as RA-L paper.

TABLE I: Comparison of lidar sensors across datasets

Dataset	Lidar Sensors Included	Type of Lidar			Focus Area
		Spinning	Solid-State	Dome	
KITTI	Velodyne HDL-64E	✓			Autonomous Driving, SLAM
Oxford RobotCar	Velodyne HDL-64E, LMS-151, LD-MRS 3D	✓			Urban Navigation, Long-Term SLAM
Ouster (2020)	OS0, OS1, OS2, OSDome	✓		✓	Sensor Benchmarking
Livox Simu-dataset	Livox Horizon, Tele-15		✓		Object Detection, SLAM
TIERS Lab Dataset	Velodyne VLP-16, Ouster OS0-128, OS1-64, Livox Horizon, Livox Avia	✓	✓		General-Purpose SLAM & Mapping
ApolloScape	Riegl VMX-1HA (VUX-1HA Laser Scanners), Velodyne HDL-64E	✓			Urban Mapping, High-Precision 3D Reconstruction
GEODE Dataset	Velodyne VLP-32C, Ouster OS1-32, Livox Avia	✓	✓		Localization under Degenerate Conditions
CTE-MLO Dataset	Ouster OS1-64, Robosense Helios 32, Robosense M1, Livox Mid-360	✓	✓	✓†	Continuous-Time Multi-Lidar Odometry
Ours (New Dataset)	Livox Avia, Ouster OS0-128, Livox Mid-360	✓	✓	✓	Lidar Variability & Point Cloud Matching

Note: † *The dome-shaped lidar (Livox Mid-360) in the CTE-MLO dataset is mounted only on the MAV platform; it is not integrated alongside spinning or solid-state LiDARs on ground vehicles.*

relevant concern to our study is that it does not incorporate dome-shaped sensors or assess point cloud matching performance in IMU-free settings.

Similarly, the CTE-MLO dataset [20] concentrates on continuous-time multi-lidar odometry, capturing field data across structured and unstructured environments. Although it integrates spinning and solid-state lidars, the dataset's organization varies by platform: for instance, Livox Mid-360 is mounted only on a MAV, while ground vehicles primarily utilize Ouster and Robosense sensors. This platform-specific variation limits direct cross-modality comparisons under consistent environmental conditions.

2) Summary: Although significant progress has been made in the development of high-end spinning lidars, cost-effective solid-state lidars, and dome-shaped lidars, existing datasets do not encompass all of these sensor types within a single data sequence, as shown in Table I. This limitation presents challenges for systematically evaluating lidar performance using state-of-the-art SLAM approaches. It is worth noting that, for example, the CTE-MLO dataset includes all these categories of lidars; however, since they are mounted on different platforms, it is not feasible to conduct a fair and unified evaluation of SLAM methods across them.

In contrast, to address this gap, our dataset integrates all these types of sensors, including the Livox Avia, Livox Mid-360, and Ouster OS-series lidars within a single data sequence and mounted on an identical robotic platform. It serves as a comprehensive benchmarking resource, enabling detailed evaluations of point cloud matching techniques in IMU-free contexts and facilitating future research into multimodal lidar integration for SLAM and 3D reconstruction applications.

C. Point Cloud Matching

Classic point cloud matching approaches include point-to-point, point-to-plane, and hybrid ICP algorithms, each tailored to specific geometric and data-quality conditions.

Point-to-point ICP minimizes the Euclidean distance between corresponding points in two point clouds via iterative optimization [21]:

$$E_{\text{p2p}}(\mathbf{R},\mathbf{t}) = \sum_{i=1}^{N} \| \mathbf{R}\mathbf{p}_i + \mathbf{t} - \mathbf{q}_i \|^2$$

where $\mathbf{p}_i$ and $\mathbf{q}_i$ are the matching points in the i-th source and target clouds, with the estimation of optimal rotation $\mathbf{R}$ and translation $\mathbf{t}$ mapping the source to the target. While efficient, this method is sensitive to noise, outliers, and sparsity.

Point-to-plane ICP refines alignment by projecting the source–target offset onto the target surface normal [22], [23]:

$$E_{\text{p2l}}(\mathbf{R},\mathbf{t}) = \sum_{i=1}^{N} \Big(\mathbf{n}_i^\top (\mathbf{R}\mathbf{p}_i + \mathbf{t} - \mathbf{q}_i) \Big)^2$$

where $\mathbf{n}_i$ is the unit normal at $\mathbf{q}_i$. This error term measures the distance of the transformed point to the tangent plane at its correspondence, improving convergence in structured environments with planar surfaces.

Hybrid ICP combines the two formulations using a convex combination of the error terms [24]:

$$E_\alpha(\mathbf{R},\mathbf{t}) = \alpha\, E_{\text{p2p}}(\mathbf{R},\mathbf{t}) + (1-\alpha)\, E_{\text{p2l}}(\mathbf{R},\mathbf{t}), \qquad \alpha \in [0,1]$$

where α balances the two objectives: $\alpha = 1$ reduces to point-to-point while $\alpha = 0$ to point-to-plane. This strategy enhances robustness in scenes with mixed geometries or varying point cloud densities.

Each variant presents trade-offs: point-to-point ICP is fast but less tolerant to irregular data; point-to-plane excels in structured settings; hybrid ICP offers flexibility by adapting to scene complexity.

III. Methodology

This section outlines the methodology for collecting, processing, and analyzing point cloud data from multiple lidars.

A. Hardware

The hardware used for the data collection in this study is illustrated in Fig. 2. The moving robot platform is a Unitree B1 quadruped robot equipped with various sensors, including Livox Mid-360 and Avia, Ouster OS0-128, RealSense L515, and Xsens MTI-680G. Table II shows the specification of the three distinct lidars.

B. Software

The software environment was built on Ubuntu 20.04 with ROS Noetic, which was the foundation for acquiring and processing sensor data. Several dependencies were integrated to enable efficient point cloud extraction, conversion, and trajectory evaluation. The EVO package [1] was utilized to compute the Absolute Pose Error (APE), providing a standardized measure of odometry accuracy. Custom Python scripts were also developed to extract, format, and analyze the odometry outputs generated by various ICP methods.

[1] https://github.com/MichaelGrupp/evo

IEEE Robotics and Automation Letters (RA-L) paper, presented at ICRA 2026, Vienna, Austria. Cite as RA-L paper.

TABLE II: Specifications of the three lidar sensors used in the study.

Sensor	Type	FoV (H × V)	Max Range (m)	Power (W)	Supply Voltage (V)	Weight (g)	IMU Model
Ouster OS0-128	Spinning	360° × 90° (nominal)	Up to 240	14–20 (28 peak)	10–51	430–500	IAM-20680HT
Livox Avia	Solid-state	70.4° × 77.2° (non-repetitive)	Up to 450	8–9 (16 peak)	10–15 (9–30 w/ conv.)	498	BMI088
Livox Mid-360	Dome-shaped	360° × (-7° to 52°)	Up to 70	6.5	9–27	265	ICM40609

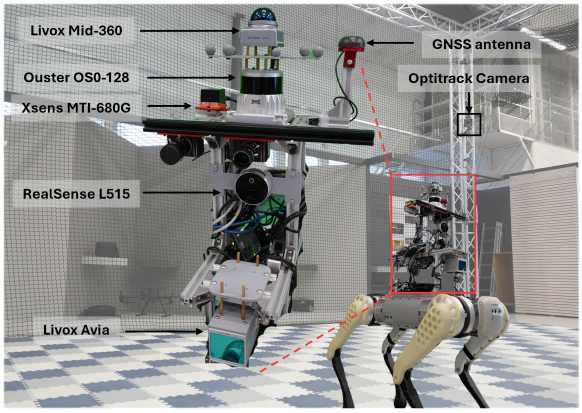

Fig. 2: The hardware used for the data collection.

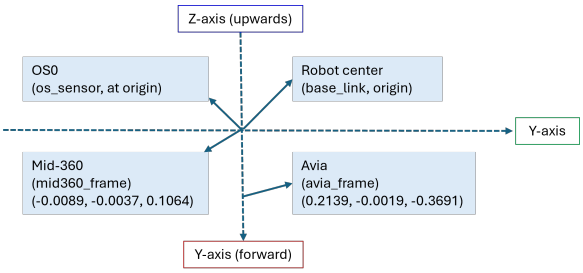

Fig. 3: The calibrated data collection platform.

C. Sensor Calibration and Synchronization

The calibration of the lidars follows the optimization-based methodology presented in [25]. During the calibration procedure, the coordinate frame of the Ouster OS0 is designated as the reference frame for all other sensors. The center of the MoCap markers is positioned at the center of the Ouster OS0 and the robot to facilitate alignment. For calibration, point cloud data were collected from the lidars within an indoor office environment while the sensor platform remained stationary. Initially, the point cloud data from each lidar was manually aligned to the reference frame through approximate transformations obtained by direct measurements. Subsequently, the Generalized Iterative Closest Point (GICP) algorithm [24] was applied to refine the relative transformations between each lidar and the reference frame. The resulting calibration outcomes are illustrated in Fig. 3.

The lidar sensors were connected via Ethernet, and temporal synchronization across all sensors was achieved using the Precision Time Protocol (PTP), owing to the absence of a hardware trigger signal. To further mitigate synchronization issues, all lidar sensor drivers and associated programs were executed locally on a high-performance computer. This synchronization strategy has been demonstrated to limit latency to less than 10 ms [17].

D. Data Collection

The sensors were rigidly mounted onto a customized sensor platform as shown in Fig. 2. Data collection was conducted across structured indoor and unstructured outdoor environments, specifically selected to challenge the lidar sensors across diverse conditions commonly encountered:

1) Indoor Environment: Indoor data collection took place within a controlled, factory-like experimental facility. A MoCap system was deployed to provide accurate ground truth with the position error reduced to below 1 mm following system calibration, enabling high-precision evaluation and validation of lidar performance in structured scenarios.

2) Outdoor Environment: Outdoor data were recorded in two settings: *OutdoorRoad*, an open road with mixed natural and urban features; and *OutdoorForest*, a forest-neighborhood corridor with dense foliage, tree trunks at various ranges, irregular ground, and frequent partial occlusions. The forest scene has strong geometric degeneracies (self-similar vegetation, intermittent canopy, limited long-range structure) and intermittent returns, which challenge scan-to-map odometry and data association. Ground truth data was acquired using the Xsens MTI-680G, which combines IMU and GNSS/RTK to provide high-frequency (100 Hz) and high-precision (position error around 1 cm according to the device specification [26]).

E. SLAM Benchmarking and Evaluation Protocol

To assess the odometry capabilities of different lidar types under realistic conditions, we benchmarked five state-of-the-art SLAM algorithms using our synchronized multi-lidar dataset. We applied a uniform maximum lidar range of 60 m for indoor data across all SLAM pipelines to simulate constrained sensing conditions typical of indoor environments. For outdoor data, we used each sensor's default maximum sensing range (Livox Avia: 450 m, Livox Mid-360: 100 m, and Ouster OS0-128: 150 m) to reflect their real-world deployment settings. These range constraints were enforced during preprocessing to ensure comparability while preserving the practical sensing capabilities of each sensor.

The selected SLAM methods represent different architectural paradigms, ranging from tightly coupled lidar-inertial odometry to graph-based global optimization. This diversity enables a balanced evaluation that highlights the strengths and limitations of local odometry, hybrid systems, and globally optimized approaches.

- **FAST-LIO2** [27]: A tightly coupled lidar-inertial odometry system that performs direct registration of raw lidar points to the map via an iterated Kalman filter. It avoids explicit feature extraction and is widely recognized for robustness and accuracy.
- **FASTER-LIO** [28]: An efficiency-optimized variant of FAST-LIO2 that leverages parallelism and incremental data structures to reduce latency.
- **S-FAST-LIO** [29]: A lightweight formulation of the FAST-LIO family designed for sparse or resource-constrained environments, emphasizing deployment efficiency while maintaining odometry quality.

IEEE Robotics and Automation Letters (RA-L) paper, presented at ICRA 2026, Vienna, Austria. Cite as RA-L paper.

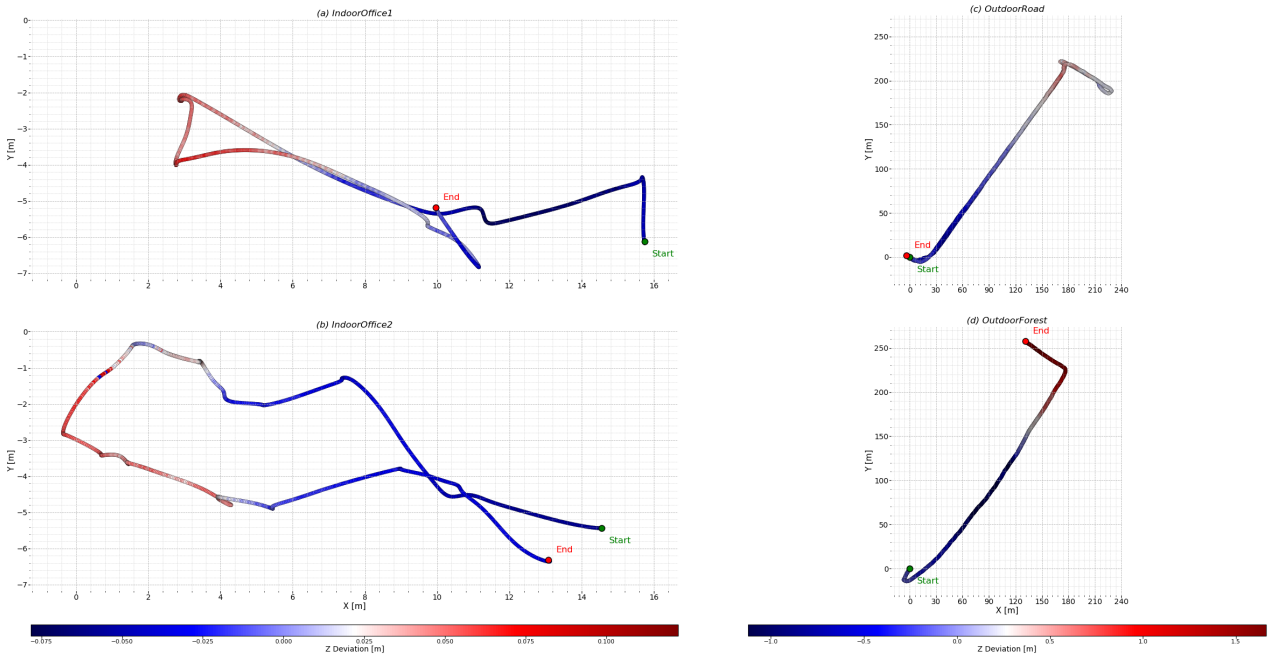

Fig. 4: The designated ground truth paths of all the collected data sequences.

- **FAST-LIO-SAM** [30]: A fused architecture that combines the high-accuracy odometry of FAST-LIO with the loop closure and factor-graph mapping backend of LIO-SAM, enabling both local precision and global consistency.
- **GLIM** [31]: A modern range-inertial SLAM framework that integrates scan-matching factors with fixed-lag smoothing and global pose graph optimization. While GLIM supports GPU acceleration for real-time performance, in our experiments, we restricted execution to the CPU to ensure a fair comparison with the FAST-LIO family, which does not rely on GPU resources. GLIM remains sensor-agnostic and is designed to be robust in degenerate scanning environments.

Together, these methods cover (i) direct scan-to-map odometry (FAST-LIO2, FASTER-LIO, S-FAST-LIO), (ii) hybrid odometry with loop closure (FAST-LIO-SAM), and (iii) globally optimized SLAM with scan matching (GLIM). By including this range of approaches, the evaluation highlights both local odometry accuracy and the benefits of loop closure and global optimization for long-term consistency.

F. Point Cloud Matching Approaches

This study evaluates three key ICP variants: Point-to-Point ICP, Point-to-Plane ICP, and Hybrid ICP, chosen for their complementary strengths in structured and unstructured environments as the representative of other point cloud matching approaches. Their suitability under different geometric scenarios is well-established in prior research [21], [22], [32].

Point-to-Point ICP minimizes the Euclidean distance between corresponding points. Though efficient, it is sensitive to outliers and sparse data. We use the KISS-ICP package, which improves robustness through adaptive thresholding and a robust kernel function for outlier suppression [33]. These enhancements make KISS-ICP particularly effective for real-time registration across diverse lidar modalities.

Point-to-Plane ICP improves alignment by incorporating local surface normals, which helps reduce geometric distortion. It is especially effective in environments rich in planar structures, such as corridors and urban settings [22]. We implemented this using Open3D-GICP [34], [35], which treats correspondences as Gaussian distributions for greater stability. Parameters such as correspondence distance and convergence thresholds were carefully tuned for each sensor.

Hybrid ICP, implemented using GenZ-ICP, blends point-to-point and point-to-plane strategies. It dynamically adjusts their weights based on scene characteristics, enhancing robustness in degenerate cases like narrow corridors [36]. This flexibility makes it suitable for heterogeneous scan patterns, such as solid-state versus spinning lidars. We evaluated GenZ-ICP across varied indoor and outdoor scenes to test its adaptability.

To ensure fair comparison, all ICP methods underwent systematic hyperparameter tuning, including settings for correspondence distance, convergence criteria, and outlier rejection. The maximum correspondence range was fixed at 20 cm for indoor data, which provided consistent accuracy across environments. For outdoor scenes, we uniformly applied a 60 m range constraint across all ICP methods to simulate short-range local registration.

Because classical ICP lacks global trajectory optimization and loop closure, we limited its evaluation to short outdoor segments, specifically *OutdoorRoad-cut0* and *OutdoorRoad-cut1*, to avoid cumulative drift and reflect its intended use case. This strategy allowed us to assess local registration performance fairly, without conflating it with long-range tracking capabilities exclusive to SLAM systems. Our results support prior findings on the importance of tuning range limits to

IEEE Robotics and Automation Letters (RA-L) paper, presented at ICRA 2026, Vienna, Austria. Cite as RA-L paper.

maintain ICP convergence stability.

G. Evaluation Metrics

Lidar-based odometry and point cloud matching accuracy were assessed by comparing the estimated trajectories to the ground-truth data. The primary metric used for this evaluation was the Absolute Pose Error (APE), which measures the deviation between the estimated and actual poses throughout the entire trajectory. For each algorithm and lidar, we report the mean and standard deviation of APE to provide insights into the accuracy and consistency of the pose estimates.

IV. Experimental Results

A. Dataset

The dataset can be found at the Github repository [2]. It is categorized into two primary subsets: indoor and outdoor environments. We collected two indoor sequences, *IndoorOffice1* and *IndoorOffice2*, featuring distinct trajectories in the same environment, and two outdoor sequences, *OutdoorRoad* and *OutdoorForest*. All data were recorded using the ROS in rosbag format. The following outlines the data format for each sensor modality included in the dataset:

Point Cloud Data: Point cloud data format varies slightly across the different lidar sensors. For the Ouster OS0 (spinning lidar), each point includes the fields `x, y, z` (`float32`), `intensity`, `reflectivity`, `ring`, `ambient`, `range` and `t` (timestamp offset in nanoseconds). In contrast, the Livox Avia and Mid-360 sensors (solid-state lidars) provide a point cloud consisting of `x, y, z, intensity`, and `tag, line` (`uint8`). Additionally, Mid-360 provides a per-point `timestamp` (`float64`) in UNIX epoch nanoseconds.

Inertial Data: IMU data is available from all lidars using the `sensor_msgs/Imu` message type. For Livox Avia and Mid-360, their IMU data are published at 200 Hz to `/avia/livox/imu` and `/mid360/livox/imu`, respectively, while for Ouster OS0, the corresponding topic is `/ouster/imu`, published at 100 Hz.

Ground Truth: Ground truth data is all in `geometry msgs::PoseStamped` format. They were obtained from a MoCap system for the indoor sequences, published under the topic `/vrpn_client_node/unitree_b1/pose`, and from a GNSS-RTK system for the outdoor sequence, available via `/gnss_pose`.

B. SLAM Benchmarking

a) Indoor SLAM Benchmark: We evaluated five SLAM algorithms across three lidars (Ouster OS0-128, Livox Avia, and Livox Mid-360) on the *IndoorOffice1* and *IndoorOffice2* datasets. The upper part of Table III reports APE as mean $\pm$ std, with underlined values indicating the best overall and bold values the best per sensor.

Livox Mid-360 achieved the best overall APE across FAST-LIO2, FASTER-LIO, and S-FAST-LIO, confirming its advantage in cluttered indoor environments. This is also reflected in Fig. 5(a), where Mid-360 (blue) shows the lowest median and tightest spread. Ouster delivered stable results with consistently narrow distributions (green), but did not dominate any single method. Livox Avia, by contrast, exhibited larger variances, particularly under GLIM, as shown by its wide red box with outliers.

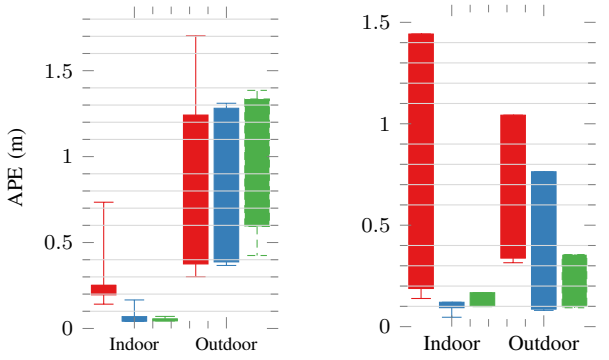

(a) SLAM (Indoor and Outdoor) (b) ICP (Indoor and Outdoor)

Fig. 5: Grouped boxplots comparing LiDAR performance across indoor and outdoor environments for SLAM and ICP. Box colors represent Avia (red), Mid-360 (blue), and Ouster (green) sensors.

b) Outdoor SLAM Benchmark: Results for the outdoor datasets are summarized in the lower part of Table III. In the *OutdoorRoad* sequence, Avia, benefiting from its 450 m range, achieved the best overall APE in one configuration (FASTER-LIO), outperforming both Livox Mid-360 and Ouster (underlined and bold value). However, it performed worse under S-FAST-LIO and GLIM, with high variance visible in Fig. 5(a). Livox Mid-360 produced strong results across multiple methods, maintaining consistency without dominating any single pipeline, while Ouster was competitive under FASTER-LIO but showed a wider error spread in the box plots.

When the more complex *OutdoorForest* sequence is included, all methods exhibit a noticeable shift toward higher APE values, as reflected in the aggregated outdoor box plots of Fig. 5(a). The red, blue, and green boxes cluster above 1 m, confirming that vegetation and occlusion amplify error accumulation across all sensors and algorithms. Thus, while OutdoorRoad highlights the benefits of Avia's long range and Ouster's structured scan, OutdoorForest reveals the limits of these advantages under canopy occlusion. Taken together, the outdoor benchmarks underscore that scene structure strongly modulates sensor strengths, and forested environments present a substantially harder challenge.

C. Point Cloud Matching Evaluation

a) Indoor Point Cloud Matching Evaluation: Three ICP pipelines (KISS-ICP, GenZ-ICP, and Open3D-GICP) were evaluated on the IndoorOffice datasets. Table IV reports APE values, with underlines for best overall and bold for per-sensor best. Mid-360 ranked best overall, particularly under KISS-ICP and GenZ-ICP on *IndoorOffice1*, and achieved competitive results under Open3D-GICP (Scan2Map) on *IndoorOffice2*. These trends are also supported by Fig. 5(b), where the compact blue box indicates low variance across indoor ICP tasks. Ouster (green) performed well in GenZ-

[2]https://github.com/TIERS/multi_modal_lidar_dataset

IEEE Robotics and Automation Letters (RA-L) paper, presented at ICRA 2026, Vienna, Austria. Cite as RA-L paper.

TABLE III: APE (mean ± std) of lidar odometry in meters for various indoor and outdoor dataset settings. For each lidar type within each data sequence, the highest accuracy is indicated in bold. The overall best performance across different lidar types is both bolded and underlined.

SLAM	***IndoorOffice1***			***IndoorOffice2***		
	Avia_10Hz	Mid360_10Hz	Ouster_10Hz	Avia_10Hz	Mid360_10Hz	Ouster_10Hz
FAST-LIO2	0.1436 ± 0.1390	0.0451 ± **0.0150**	0.0446 ± **0.0298**	0.3581 ± 0.1334	0.0412 ± 0.0201	0.0438 ± 0.0471
FASTER-LIO	**0.1223** ± **0.0517**	0.0918 ± 0.0423	0.0571 ± 0.0304	0.2692 ± 0.1386	0.0460 ± **0.0147**	0.0549 ± 0.0491
S-FAST-LIO	0.1808 ± 0.1840	**0.0427** ± 0.0161	0.0541 ± 0.0367	**0.1019** ± **0.0536**	**0.0388** ± 0.0190	0.0504 ± 0.0529
GLIM	0.3104 ± 0.2461	0.1760 ± 0.1734	0.0733 ± 0.0395	1.1587 ± 0.6535	0.1559 ± 0.1142	0.0668 ± 0.0559
FAST-LIO-SAM	0.1436 ± 0.1392	0.0457 ± 0.0153	**0.0442** ± 0.0299	0.3581 ± 0.1327	0.0400 ± 0.0190	**0.0431** ± **0.0398**
SLAM	***OutdoorRoad***			***OutdoorForest***		
FAST-LIO2	0.3755 ± 0.1527	0.3893 ± 0.1788	0.5845 ± 0.3127	**1.2309**± 0.7778	1.2813 ± 0.8441	1.3394 ± 0.7502
FASTER-LIO	**0.3013** ± **0.0818**	**0.3666** ± 0.1668	**0.4245** ± **0.2273**	1.2453 ± **0.7512**	1.3064 ± 0.8120	**1.2392** ± **0.7277**
S-FAST-LIO	0.6730 ± 0.3205	0.3721 ± **0.1641**	0.6223 ± 0.3282	1.2418 ± 0.8039	**1.2637** ± **0.8167**	1.3854 ± 0.7539
GLIM	1.7026 ± 0.2774	0.6867 ± 0.5828	0.8303 ± 0.4314	N/A	N/A	1.3225 ± 0.7449
FAST-LIO-SAM	0.3700 ± 0.1545	0.3873 ± 0.1775	0.5795 ± 0.3137	1.2376 ± 0.7723	1.3104 ± 0.8442	1.3522 ± 0.7363

TABLE IV: Absolute Pose Error (APE) across ICP methods and lidars for indoor and outdoor data (mean ± std, in meters). For each lidar type within each data sequence, the highest accuracy is indicated in bold. The overall best performance across different lidar types is both bolded and underlined.

Method	***IndoorOffice1***			***IndoorOffice2***		
	Avia_10Hz	Mid360_10Hz	Ouster_10Hz	Avia_10Hz	Mid360_10Hz	Ouster_10Hz
KISS-ICP	**0.1348** ± **0.1049**	**0.0483** ± **0.0405**	0.1042 ± 0.0838	0.6945 ± 0.2825	**0.0441** ± **0.0286**	0.0996 ± 0.0782
GENZ-ICP	0.2639 ± 0.1527	0.0653 ± 0.0588	**0.0937** ± **0.0511**	**0.1121** ± 0.0868	0.1214 ± 0.0586	**0.1037** ± **0.0764**
Open3D-GICP (Scan2Map)	0.1387 ± 0.0738	0.1115 ± 0.0491	0.1082 ± 0.0613	0.1387 ± **0.0592**	0.0899 ± 0.0425	0.1648 ± 0.0989
Open3D-GICP (Scan2Scan)	1.4341 ± 0.2804	0.1057 ± 0.0574	0.1161 ± 0.0524	1.4504 ± 0.9441	0.1345 ± 0.0787	0.2182 ± 0.1498
	OutdoorRoad-cut0			***OutdoorRoad-cut1***		
KISS-ICP	0.3917 ± 0.3135	**0.0545** ± **0.0424**	**0.0787** ± **0.0502**	**0.2840** ± **0.2149**	0.1058 ± 0.0628	0.1072 ± 0.0559
GENZ-ICP	**0.1924** ± **0.1046**	0.0645 ± 0.0489	0.0810 ± 0.1157	0.4376 ± 0.2479	0.1081 ± **0.0490**	0.1157 ± 0.0603
Open3D-GICP (Scan2Map)	0.7787 ± 0.7435	0.0855 ± 0.0534	0.1177 ± 0.0655	0.8137 ± 0.4766	**0.0953** ± 0.0513	**0.0803** ± **0.0549**
Open3D-GICP (Scan2Scan)	1.0489 ± 0.9901	1.0316 ± 0.3959	0.2015 ± 0.0900	1.0357 ± 0.8246	0.4952 ± 0.2269	0.5075 ± 0.2780

ICP and Open3D-GICP, but showed a slightly wider spread. Avia (red) consistently lagged, particularly in Open3D-GICP (Scan2Scan), where its sparse vertical resolution resulted in high errors and variance.

b) Outdoor Point Cloud Matching Evaluation: We benchmarked the same ICP pipelines on *OutdoorRoad-cut0* and *OutdoorRoad-cut1* using a 60 m range. Table IV shows the APE statistics. Mid-360 consistently ranked best or near-best across all pipelines. It achieved the lowest APE in Open3D-GICP (Scan2Map) on *OutdoorRoad-cut1*, and also led in GenZ-ICP and KISS-ICP on *OutdoorRoad-cut0*. Its tight blue box plot in Fig. 5(b) confirms low variance outdoors. Ouster (green) performed best under Open3D-GICP (Scan2Map) on *OutdoorRoad-cut1* and showed strong stability under KISS-ICP in *OutdoorRoad-cut0*, but its advantages were method-specific. Avia (red) underperformed across all outdoor ICP configurations, often showing the highest errors and variances, particularly under Open3D-GICP (Scan2Scan).

D. Discussion

Overall performance patterns. Across all datasets, the FAST-LIO family (FAST-LIO2, FASTER-LIO, S-FAST-LIO) achieved the lowest errors and most stable odometry. FAST-LIO-SAM added robustness on long sequences through loop closure, while GLIM underperformed under our CPU-only evaluation.

Impact of lidar modality. Sensor geometry strongly shaped results. The Livox Mid-360, with its wide vertical FoV and non-repetitive pattern, consistently provided stable performance indoors and remained competitive outdoors. The Livox Avia, benefiting from long-range returns, excelled in road-like environments, but its advantage diminished under occlusion. The Ouster OS0-128 performed reliably in structured settings but showed greater variability in cluttered scenes.

Algorithm–sensor interplay. Direct scan-to-map pipelines in the FAST-LIO family adapted well to the irregular Livox sampling, enabling both Avia and Mid-360 to remain competitive with the Ouster. Mid-360's vertical coverage benefited cluttered environments, while Avia's long-range returns were most useful in open settings. GLIM produced stable results with Ouster outdoors but repeatedly failed to complete with Livox sensors in the most challenging cases, highlighting the importance of algorithm–sensor compatibility.

Environmental factors and practical implications. The dataset confirms how environmental structure amplifies or suppresses sensor strengths: vertical coverage dominates indoors, long-range visibility is critical on roads, and canopy occlusion raises errors across all modalities in forests. Taken together, these results suggest that FAST-LIO variants remain strong defaults across environments, with FAST-LIO-SAM being preferred when global consistency is required. More importantly, the dataset now enables exploration of multi-lidar fusion, where Mid-360's coverage, Avia's range, and Ouster's structured scan could be exploited complementarily.

V. Conclusion

This study addresses the heterogeneity of lidar sensor types by introducing a novel dataset that, for the first time, includes data collected using three distinct categories of lidars: dome-shaped solid-state lidar, limited FoV solid-state lidar, and spinning lidar. The dataset contains both indoor and outdoor environments with ground truth provided using MoCap in indoor settings and GNSS-RTK in outdoor scenarios. In addition to the dataset, we present a comprehensive SLAM benchmarking across all data sequences, utilizing multiple state-of-the-art SLAM algorithms. Results showed that the Livox Mid-360 consistently delivered high accuracy and stability across ICP and SLAM methods, particularly in complex scenes, owing to its wide vertical field of view and dense scan coverage. Livox Avia performed well in long-range SLAM scenarios but exhibited limitations in local registration. Ouster sensors achieved competitive results, especially under spinning-optimized SLAM pipelines, though their limited vertical resolution reduced performance in semi-structured environments. Furthermore, to investigate the impact of lidar variability on geometric registration, we evaluate the point cloud matching performance of different lidars using several ICP (Iterative Closest Point) variants, without incorporating IMU assistance. Results suggest that the Mid-360 consistently achieves the most accurate alignment across a variety of test cases.

References

[1] Jiaqiang Zhang, Xianjia Yu, Ha Sier, Haizhou Zhang, and Tomi Westerlund. Event-based sensor fusion and application on odometry: A survey. In *2025 IEEE 6th International Conference on Image Processing, Applications and Systems (IPAS)*, pages 1–6. IEEE, 2025.

[2] Chunge Bai, Tao Xiao, Yajie Chen, Haoqian Wang, Fang Zhang, and Xiang Gao. Faster-lio: Lightweight tightly coupled lidar-inertial odometry using parallel sparse incremental voxels. *IEEE Robotics and Automation Letters*, 7(2):4861–4868, 2022.

[3] Danni Wu, Zichen Liang, and Guang Chen. Deep learning for lidar-only and lidar-fusion 3d perception: A survey. *Intelligence & Robotics*, 2(2):105–129, 2022.

[4] Dongjiao He, Wei Xu, Nan Chen, Fanze Kong, Chongjian Yuan, and Fu Zhang. Point-lio: Robust high-bandwidth light detection and ranging inertial odometry. *Advanced Intelligent Systems*, 5(7):2200459, 2023.

[5] Jiarong Lin and Fu Zhang. Loam livox: A fast, robust, high-precision lidar odometry and mapping package for lidars of small fov. In *2020 IEEE international conference on robotics and automation (ICRA)*, pages 3126–3131. IEEE, 2020.

[6] Xiao Zhang, Zhanhong Huang, Garcia Gonzalez Antony, Witek Jachimczyk, and Xinming Huang. Stream-based ground segmentation for real-time lidar point cloud processing on fpga, 2024.

[7] Sier Ha, Honghao Du, Xianjia Yu, Jian Song, and Tomi Westerlund. Enhancing the reliability of lidar point cloud sampling: A colorization and super-resolution approach based on lidar-generated images. *arXiv preprint arXiv:2409.11532*, 2024.

[8] Haizhou Zhang, Xianjia Yu, Sier Ha, and Tomi Westerlund. Lidar-generated images derived keypoints assisted point cloud registration scheme in odometry estimation. *Remote Sensing*, 15(20):5074, 2023.

[9] Ha Sier, Xianjia Yu, Iacopo Catalano, Jorge Pena Queralta, Zhuo Zou, and Tomi Westerlund. Uav tracking with lidar as a camera sensor in gnss-denied environments. In *2023 International Conference on Localization and GNSS (ICL-GNSS)*, pages 1–7. IEEE, 2023.

[10] Xianjia Yu, Sahar Salimpour, Jorge Pena Queralta, and Tomi Westerlund. General-purpose deep learning detection and segmentation models for images from a lidar-based camera sensor. *Sensors*, 23(6):2936, 2023.

[11] Tao Yin, Jingzheng Yao, Yan Lu, and Chunrui Na. Solid-state-lidar-inertial-visual odometry and mapping via quadratic motion model and reflectivity information. *Electronics*, 12(17), 2023.

[12] Loris Redovniković, Antun Jakopec, Janusz Będkowski, and Jurica Jagetić. The affordable diy mandeye lidar system for surveying caves, and how to convert 3d clouds into traditional cave ground plans and extended profiles. *International Journal of Speleology*, 53(3):7, 2025.

[13] Andreas Geiger, Philip Lenz, Christoph Stiller, and Raquel Urtasun. Vision meets robotics: The kitti dataset. *International Journal of Robotics Research (IJRR)*, 2013.

[14] Will Maddern, Geoff Pascoe, Chris Linegar, and Paul Newman. 1 Year, 1000km: The Oxford RobotCar Dataset. *The International Journal of Robotics Research (IJRR)*, 36(1):3–15, 2017.

[15] Peng Wang, Xinyu Huang, Xinjing Cheng, Dingfu Zhou, Qichuan Geng, and Ruigang Yang. The apolloscape open dataset for autonomous driving and its application. *IEEE transactions on pattern analysis and machine intelligence*, 2019.

[16] Ouster_copyright. Ouster dataset, 2020.

[17] Qingqing Li, Xianjia Yu, Jorge Peña Queralta, and Tomi Westerlund. Multi-modal lidar dataset for benchmarking general-purpose localization and mapping algorithms. *arXiv preprint arXiv:2203.03454*, 2022.

[18] Livox_copyright. Livox dataset, 2020.

[19] Zhiqiang Chen, Yuhua Qi, Dapeng Feng, Xuebin Zhuang, Hongbo Chen, Xiangcheng Hu, Jin Wu, Kelin Peng, and Peng Lu. Heterogeneous lidar dataset for benchmarking robust localization in diverse degenerate scenarios, 2024.

[20] Hongming Shen, Zhenyu Wu, Yulin Hui, Wei Wang, Qiyang Lyu, Tianchen Deng, Yeqing Zhu, Bailing Tian, and Danwei Wang. Cte-mlo: Continuous-time and efficient multi-lidar odometry with localizability-aware point cloud sampling, 2025.

[21] P.J. Besl and Neil D. McKay. A method for registration of 3-d shapes. *IEEE Transactions on Pattern Analysis and Machine Intelligence*, 14(2):239–256, 1992.

[22] Y. Chen and G. Medioni. Object modeling by registration of multiple range images. In *Proceedings. 1991 IEEE International Conference on Robotics and Automation*, pages 2724–2729 vol.3, 1991.

[23] Kok-Lim Low. Linear least-squares optimization for point-to-plane icp surface registration. *Chapel Hill, University of North Carolina*, 4(10):1–3, 2004.

[24] Aleksandr Segal, Dirk Haehnel, Sebastian Thrun, et al. Generalized-icp. In *Robotics: science and systems*, volume 2, page 435. Seattle, WA, 2009.

[25] Jinyong Jeong, Younggun Cho, Young-Sik Shin, Hyunchul Roh, and Ayoung Kim. Complex urban lidar data set. In *2018 IEEE international conference on robotics and automation (ICRA)*, pages 6344–6351. IEEE, 2018.

[26] Movella. Mti-680g. https://www.xsens.com/hubfs/Downloads/Leaflets/MTi-680G.pdf. [Online] - Last access: 2025-10-1.

[27] Wei Xu, Yixi Cai, Dongjiao He, Jiarong Lin, and Fu Zhang. Fast-lio2: Fast direct lidar-inertial odometry. *IEEE Transactions on Robotics*, 38(4):2053–2073, 2022.

[28] Chunge Bai, Tao Xiao, Yajie Chen, Haoqian Wang, Fang Zhang, and Xiang Gao. Faster-lio: Lightweight tightly coupled lidar-inertial odometry using parallel sparse incremental voxels. *IEEE Robotics and Automation Letters*, 7(2):4861–4868, 2022.

[29] Zlwang7. A simplified implementation of fast_lio, 2023.

[30] Mason Lee Eungchang and Cattaneo Daniele. Fast-lio-sam: A slam implementation combining fast-lio2 with pose graph optimization and loop closing based on lio-sam. https://github.com/engcang/FAST-LIO-SAM, 2023. Accessed: 2026-03-07.

[31] Kenji Koide, Masashi Yokozuka, Shuji Oishi, and Atsuhiko Banno. Glim: 3d range-inertial localization and mapping with gpu-accelerated scan matching factors. *Robotics and Autonomous Systems*, 179:104750, 2024.

[32] Zhengyou Zhang. Iterative point matching for registration of free-form curves and surfaces. *International journal of computer vision*, 13(2):119–152, 1994.

[33] Ignacio Vizzo, Tiziano Guadagnino, Benedikt Mersch, Louis Wiesmann, Jens Behley, and Cyrill Stachniss. Kiss-icp: In defense of point-to-point icp – simple, accurate, and robust registration if done the right way. *IEEE Robotics and Automation Letters*, 8(2):1029–1036, February 2023.

[34] Qian-Yi Zhou, Jaesik Park, and Vladlen Koltun. Open3D: A modern library for 3D data processing. *arXiv:1801.09847*, 2018.

[35] Edo Jelavic, Julian Nubert, and Marco Hutter. Open3d slam: Point cloud based mapping and localization for education. In *Robotic Perception and Mapping: Emerging Techniques, ICRA 2022 Workshop*, page 24. ETH Zurich, Robotic Systems Lab, 2022.

[36] Daehan Lee, Hyungtae Lim, and Soohee Han. Genz-icp: Generalizable and degeneracy-robust lidar odometry using an adaptive weighting. *IEEE Robotics and Automation Letters*, 10(1):152–159, January 2025.